ResearchGate

See discussions, stats, and author profiles for this publication at: https://www.researchgate.net/publication/267097707

Intrinsically Conductive Organo−Silver Linear Chain Polymers [−S−Ag−S−Biphenyl−] n Assembled on Roughened Elemental Silver

ARTICLE *in* THE JOURNAL OF PHYSICAL CHEMISTRY C · OCTOBER 2014

Impact Factor: 4.77 · DOI: 10.1021/jp505441k

CITATION
1

READS
34

7 AUTHORS, INCLUDING:

Shirshendu Dey
University of California, Irvine
15 PUBLICATIONS **28** CITATIONS
SEE PROFILE

Nicholas Tallarida
University of California, Irvine
4 PUBLICATIONS **7** CITATIONS
SEE PROFILE

Vartkess Ara Apkarian
University of California, Irvine
193 PUBLICATIONS **4,101** CITATIONS
SEE PROFILE

Available from: Vartkess Ara Apkarian
Retrieved on: 26 January 2016

THE JOURNAL OF PHYSICAL CHEMISTRY C

Article

pubs.acs.org/JPCC

Intrinsically Conductive Organo−Silver Linear Chain Polymers [−S−Ag−S−Biphenyl−]$_n$ Assembled on Roughened Elemental Silver

Stephen S. Sasaki,[∥,†] Yan-Ning Zhang,[§,‡] Shirshendu Dey,[†] Nicholas Tallarida,[†] Patrick Z. El-Khoury,[⊥,†] V. A. Apkarian,*[,†] and Ruqian Wu*[,‡]

[†]Department of Chemistry and [‡]Department of Physics and Astronomy, University of California, Irvine, California 92697-4575, United States

Supporting Information

ABSTRACT: A combined experimental and theoretical study of the facile polymerization of biphenyl-4,4′-dithiol (BPDT) to form intrinsically conductive linear chain [−Ag−S−BP−S−]$_n$ polymers is described. BPDT readily polymerizes and extrudes on roughened surfaces of elemental silver under ambient conditions. The self-assembled polymers can be sharply imaged through scanning electron microscopy because of their silver content and conductivity. Cyclic current versus voltage measurements (I/V curves) using a scanning tunneling microscope establish that the conductivity is intrinsic, consistent with the metallic conductivity of the linear polymer predicted through density functional theory. Systematic calculations identify that the roughness-catalyzed polymerization is driven by mobile Ag adatoms and adatom-mobilized monomers.

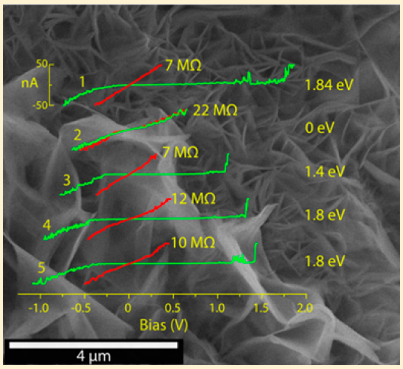

INTRODUCTION

Although conductive organic polymers are in common use in a wide array of technological applications, developments in novel composition and synthesis continue to optimize performance, processability, and stability.[1−4] The major advance in this field was made by the discovery that the modest intrinsic conductivity of organic polymers (<10^{-3} S/m) could be dramatically enhanced by 6−7 orders of magnitude through oxidative or reductive doping.[5,6] Stable polymers with high intrinsic conductivity remain desirable. Carbon nanotubes and graphitic sheets have been advanced for this purpose, although with limited utility because of their poor processability.[7,8] An alternative design motif is provided by nanostructured arrays of metallo−organic polymers, in which conductivity as high as 10^4 S/m has been reached.[9] Ultimately, molecular wires and sheets are sought for applications such as bottom-up fabrication of molecular electronics.[10] Here, we report the discovery of a conductive organo−silver polymer which can be suitably processed as molecular wires and sheets.

In the course of preparing self-assembled monolayers (SAM) of biphenyl-4,4′-dithiol (BPDT) on electrochemically etched silver tips, in contrast to uniform SAMs that form on flat gold or silver surfaces,[11] we discover large-scale (>1 μm) growth of surface-assembled polymers (SAPs). The polymerization takes place upon dipping roughened silver metal in a solution containing BPDT. There are no other requirements, as we describe in the Polymer Synthesis section below. Because of their silver content, the polymers can be sharply imaged through scanning electron microscopy (SEM), as illustrated in Figure 1. Moreover, the SEM contrast does not fade with extended exposure to electron beam bombardment, which indicates that the organo−silver polymers are conductive. The observed distinct habits can be loosely associated with the roughness landscape of the electrochemically etched silver surface, which shows great variation with processing, as illustrated in Figure 1. Through energy-dispersive X-ray spectroscopy (EDS) and X-ray photoelectron spectroscopy (XPS), we establish the elemental composition of the SAP to be consistent with that of linear [−Ag−S−BP−S−]$_n$. Matrix-assisted laser desorption ionizations mass spectrometry (MALDI) establishes the mean chain length of the covalently linked polymers to be greater than 500 units. Raman spectroscopy of the SAPs on silver shows evidence for both −S−S− and −S−Ag−S− linkage. However, quantitative structural information could not be extracted from Raman, as described in the Supporting Information. Below, we describe the cyclic conductivity measurements using scanning tunneling microscopy (STM) that rigorously establish the intrinsic, through-bond conductivity of the SAP. We then discuss our density functional theory (DFT) calculations that predict metallic conductivity for linear −S−Ag−S− linkages and clarify the key steps in the heterogeneous polymerization of Ag−BPDT. In effect, surface roughness catalyzes the efficient copolymerization of the dithiol and zerovalent silver under ambient conditions.

Special Issue: John C. Hemminger Festschrift

Received: June 2, 2014
Revised: October 19, 2014

 © XXXX American Chemical Society dx.doi.org/10.1021/jp505441k | J. Phys. Chem. C XXXX, XXX, XXX−XXX

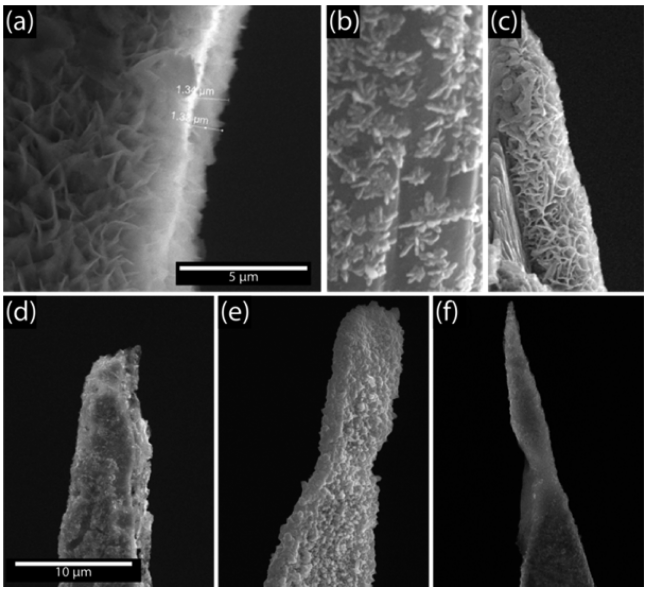

Figure 1. SEM images of common growth patterns of the organo–silver polymer on etched silver wires: (a) sheets, (b) filaments, and (c) corals. Electrochemically etched silver wires develop roughness on many scales. Examples are shown in panels d–f, without implying a correlation between polymer habit and surface morphology. The indicated scales apply for the three images in each row.

EXPERIMENTAL SECTION

Polymer Synthesis. Freshly etched silver wire is dipped (1 s × 2 cycles) in HF to rid the surface of oxides and/or other residues produced from the etching process. The tip is then sonicated in ethanol and suspended in the neat solvent for 20 min. Subsequent sonication with fresh solvent was repeated three times. Following sonication and washing, the tip is immersed in a homogeneous saturated BPDT solution and suspended for 24–48 h. After polymer growth, the tip is sonicated in neat ethanol for 30 min and washed rigorously to ensure the removal of any residues. The resulting tip is allowed to dry prior to SEM/EDS/Raman measurements. This is the standard procedure that produces the sheeted structure seen in Figure 1A. We establish the following:

(a) Oxygen does not play a role in the catalytic polymerization. The procedure could be completely reproduced in a Schlenk line, under oxygen-free conditions.
(b) The solvent does not play a role in the chemistry. The same polymerization is observed using a saturated solution of BPDT in ethanol or 1 mM solutions of BPDT in toluene.
(c) The chemistry does not occur on gold. On gold wires, the same procedure forms a smooth SAM, which does not grow beyond a monolayer. Neither SAMs nor polymers are observed on inert aluminum surfaces.
(d) The polymerization is inhibited on heavily oxidized silver surfaces. Polymer growth occurs upon immersing untreated silver wires, as purchased, in a saturated BPDT ethanol solution. After the metal wire is suspended in the solution for 24 h, the polymer is visible under SEM. However, the surface coverage is significantly lower than what is observed on cleaned surfaces.
(e) Clean, roughened silver surfaces accelerate the polymerization. This is demonstrated by monitoring the growth of the polymer on a silver foil, with adjacent polished and mechanically roughened areas. The coverage and growth rate is dramatically larger on the roughened surface.
(f) The habit of the polymer is determined by the morphology of defects (roughness). The dendritic polymer flowers (Figure 1b), which show directed growth of bundled strands, underscore this observation. The silver surface is bare where smooth, while polymer growth is initiated and perpetuated at single nucleation sites. The dense coral structure (Figure 1c) and the more open sheet structure (Figure 1a) occur in large separate domains on a single wire, subject to the same history of preparation. Because silver atoms are incorporated in the polymer, the defects must sustain the supply of atoms as the polymer grows.

Polymer Characterization. Electron transfer through the Ag–DBDT polymer was investigated using an ambient STM (NT-MDT). The characteristic current–voltage (I/V) curves were measured using a gold tip. The feedback is momentarily interrupted to perform the I/V scan. In repeated scans, the

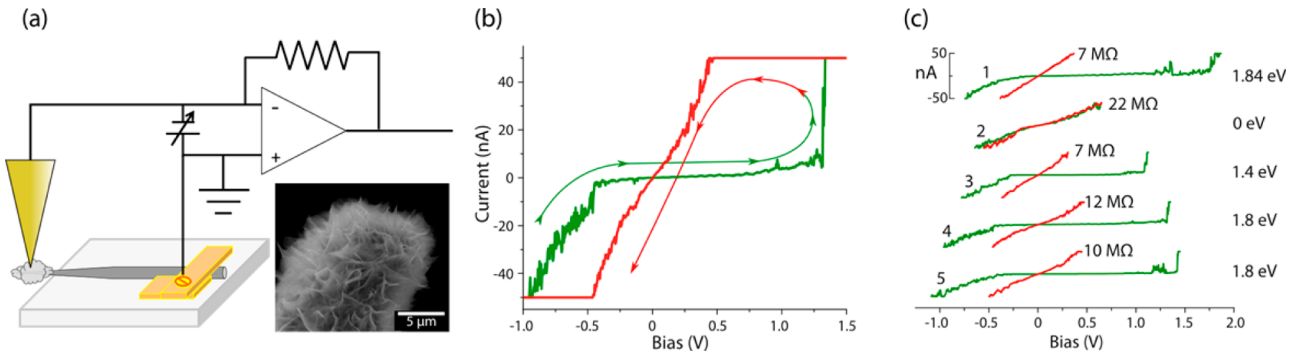

Figure 2. Conductivity measurements. (a) An ambient STM equipped with a gold tip is used to measure the conductivity of self-assembled polymers on an electrochemically etched silver wire. (inset) An SEM image shows the polymer coverage on the etched portion of the silver wire. (b) Cyclic I/V measurements are used to characterize the polymer's electrical properties. (c) Five consecutive cyclic I/V measurements show the variation in junction resistance (center) and bandgap of the insulating state (right). The runs indicate an insulating state with a bandgap of 1.8 eV, which switches to metallic conductivity near 1.4 V. The transition is ascribed to making electrical contact with the gold tip through covalent S–Au bonding. The behavior is highly reproducible, as indicated by the set of scans in panel c. The variations in the resistance, obtained from the slopes dI/dV at $V = 0$, are associated with variations in the length of the interrogated polymer, as measured by the variation in displacement of $\delta z \sim 100$ nm of the gold tip relative to the silver electrode.

dx.doi.org/10.1021/jp505441k | J. Phys. Chem. C XXXX, XXX, XXX–XXX

feedback is turned on between scans to compensate for any change in tunneling distance due to mechanical instabilities of the tunnel junction. The sample is grounded, and bias is applied to the STM tip. Tips were prepared by electrochemically etching 350 μm Au wire, in a procedure that typically yields tip cones of ~50−100 nm diameter.[28]

Energy-dispersive X-ray spectroscopy was performed on BPDT SAPs extending far enough from the metal surface to avoid any contribution from the bulk silver (Figure 2). Measurements were also carried out on 20 different ~1 μm^2 areas of the stripped polymer, using graphite tape to strip it from the silver wire. All sampled areas on the wire and on the stripped polymer show nearly identical ratios of S:Ag = 2:1. The silver is homogeneously distributed in the polymer. The mean atom ratio seen when imaging the silver surface is ⟨C:Ag⟩ ~ 11:1, which can be regarded to be in agreement with the 12:1 ratio expected for Ag−DBDT. The elemental composition suggests a structure entirely composed of covalent −S−Ag−S− linkage. EDS measurements show no evidence of oxidation on silver needles coated by the polymer over several weeks of aging under ambient conditions.

X-ray photoelectron spectroscopy for chemical analysis was carried out on polymers grown on mechanically roughened silver foil. In addition to S, C, and Ag, the coated foils show clear evidence of extensive oxidation, with O:S:Ag atom ratio of 1:1:0.3. A large distribution of sulfur binding sites is seen on these samples, consistent with a variety of oxidation states of sulfonates.[29] Given the absence of oxidation of SAPs on electrochemically etched needles, we conclude that the oxidation in the case of the foils was due to poor coverage. The observed elemental composition of S:Ag 2.8:1 is not inconsistent with the EDS results of 2:1. Unlike the EDS measurements, which are carried out on the isolated polymer, all contaminants of the partially oxidized silver surface are observed in the XPS measurements. The silver $3d_{5/2}$ and $3d_{3/2}$ lines observed in XPS show negligible shift in their binding energy, consistent with Ag^0, Ag_2S, and Ag_2O.[30] It is worth noting that the binding energy shifts of Ag(d)-lines are generally small.

Matrix-assisted laser desorption ionization mass spectrometry could be performed directly on polymers grown on silver foil. In this measurement a tightly focused laser ablates the material to introduce it in the mass spectrometer. The measurements establish that the polymer consists of covalently bonded long chains, with more than 500 units on average.

Computational Details. Density functional calculations were performed using the Vienna ab initio simulation package (VASP)[31] along with the projector augmented wave (PAW) method.[32] Both the generalized gradient approximation (GGA) functional[33] and the optB86b version of van der Waals density functional (vdW-DF)[34] were used to describe the exchange-correlation interaction among electrons. We used an energy cutoff of 400 eV for the plane-wave basis expansion, and a cell-size-dependent k-point mesh in the Brillouin zone (BZ) for k-space integrations. The free BPDT molecule was placed in a 40 × 20 × 20 $Å^3$ box to avoid interactions among periodic images. The Ag(111) substrate was modeled by a three-layer slab with a (6 × 6) supercell in the lateral plane, and a ~15 Å thick vacuum region was inserted between two adjacent slabs. The size of the supercell was fixed according to the lattice constant of bulk Ag (a = 4.086 Å). While atoms in the bottommost Ag layers were kept at their ideal bulk positions, positions of other Ag atoms and BPDT molecules were fully optimized until forces on them became less than 0.02 eV/Å.

RESULTS AND DISCUSSION

Conductivity. Conductivity measurements were carried out with an ambient STM on a densely packed polymer prepared on an electrochemically etched Ag wire (Ø = 500 μm). The experimental arrangement is shown in Figure 2a. An atomically sharp gold tip, with an apex cone radius of ~20 nm, is used as the STM tip. Current across the polymer is measured with the gold tip and silver wire serving as electrodes. The tip is biased relative to the grounded silver wire, and cyclic current versus voltage (I/V) curves are recorded. A typical cyclic I/V curve is shown in Figure 2b. The bias is ramped from negative to positive values, then reversed, and scanned over the same range to complete the cycle. The dramatic hysteresis seen in the I/V scan is reproducible, as illustrated by the repeated measurements shown in Figure 2c. The forward cycle reveals an insulating state, with a highest occupied molecular−lowest unoccupied molecular orbital gap of ~1.8 eV, which shows little variation with tip placement. Near +1.3 V, the current saturates abruptly at the instrument limit of 50 nA, as electrical contact is established between the gold tip and the polymer. The current remains saturated on the reverse cycle (red curve) down to +0.5 V and shows nearly ohmic response in the ±0.5 V window. The hysteretic curves are characteristic for switching between insulating and conductive states by the formation and breaking of a covalent S−Au bond at the gold−polymer junction.[12] The breaking of the bond occurs between cycles because of motion of the tip upon momentarily activating the feedback. The exception is scan 2, where the conductive state is reproduced on forward and backward scans, signifying that the electrical contact between molecule and electrodes remained intact between cycles. The hysteretic curves uniquely establish that the ohmic conductance is intrinsic; it is realized when current is injected through bonds, through covalent contacts between the silver and gold electrodes. The current in the insulating state, which is nearly 3 orders of magnitude smaller, represents the extrinsic bulk conductance.

It is possible to obtain a crude estimate of the intrinsic conductivity of the polymer. The effective resistance, given by the slope of the I/V curve at V = 0, ranges between 7 and 22 MΩ. Between the cyclic scans the tip moves with typical vertical displacements of $\delta z = \pm$ 100 nm. This variation is consistent with the SEM image, which shows surface corrugation δz ~ 500 nm over a lateral displacement of 1 μm (see Figure 2 inset). All else being the same, associating the observed variations in resistance δR = 1−10 MΩ with the correlated variations in junction gap δz = 100 nm, a conductance of $\delta(1/R)/\delta z$ = 1−10 S/m can be inferred. This is significantly higher than the best organic polymers, e.g., trans-polyacetylene, which has an intrinsic conductivity of 10^{-3}−10^{-2} S/m.[13] The latter is comparable to what is observed in the insulating state in the present. While it is tempting to assign the observed current to single molecule contacts, it is likely that many contacts are made during the switch in the I/V curve. In either case, we may conclude that the organo−silver polymers exhibit unusually large intrinsic conductivity.

Theoretical Analysis. The computed structural properties that are key to characterizing BPDT polymers assembled through −S−S− or −S−Ag−S− linkage are summarized in Figure 3. The optimized structure of the free BPDT molecule is depicted in Figure 3a. The calculated S−H bond length (b_{S-H})

dx.doi.org/10.1021/jp505441k | J. Phys. Chem. C XXXX, XXX, XXX−XXX

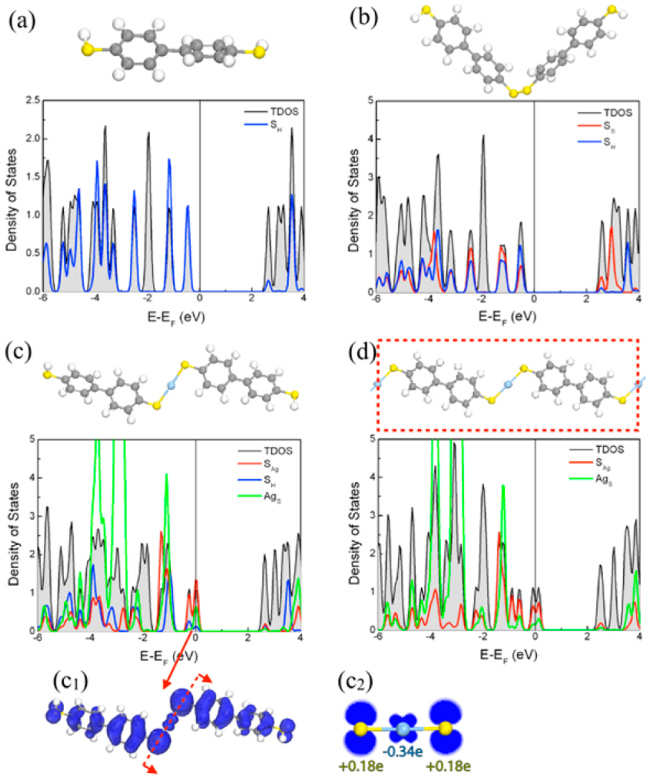

Figure 3. Optimized configurations of (a) a free single BPDT molecule, (b) two BPDT molecules with −S−S− linkage, (c) two BPDT molecules with −S−Ag−S− linkage, and (d) periodic BPDT chain connected by Ag atoms ($[-Ag-S-BP-S-]_n$). (c1) and (c2) show the top-view and side-view of the wave function of the state at the Fermi level in the free −S−Ag−S− linkage. The β charges on the Ag and S atoms are indicated in (c2). The yellow, gray, white, and cyan balls in structural models represent sulfur, carbon, hydrogen, and Ag atoms, respectively. The red dashed rectangle in panel d depicts the supercell of the $[-Ag-S-BP-S-]_n$ chain. The corresponding total density of states (TDOS) and projected density of states (PDOS) of S and/or Ag atoms are shown in the lower panel. The zero energy is at the Fermi level. The TDOS curves are scaled by a factor of 0.1 for plotting convenience.

is 1.35 Å, the C−C bond length (b_{C-C}) is 1.48 Å, and the torsion angle (φ) between the phenyl planes is 33.5° using the vdW-DF functional. The latter is closer to the experimental X-ray result of 36.4°[14] than the previous DFT calculation of 44.9°.[15] This may be fortuitous because torsion angles are rather sensitive to local environment, and the isolated molecule calculations can be expected to deviate from those observed in crystals. The total density of states (TDOS) and the projected density of states (PDOS) of the sulfur atom in Figure 3a show that the molecule is a typical insulator with an energy gap of ~2.43 eV. As building blocks, we consider dimers linked by either an S−S bond as in Figure 3b, or −S−Ag−S− chain, as in Figure 3c. We used ab initio molecular dynamics (AIMD) simulations at the GGA level to determine these structures, starting from several initial configurations with random angles between the two molecules. We first relax the system at 300 K for 1.5 ps to reach thermal equilibrium, and then cool the system to 100 K with a rate of 2×10^{13} K/s. The structures obtained at the end of the AIMD procedures are further optimized at 0 K using the vdW-DF functional. The S−S linked dimer forms a "bent" structure, with b_{S-S} = 2.03 Å, and an energy gap nearly identical to that of the monomer, as shown in Figure 3b. The silver linked dimer is linear, with b_{S-Ag} = 2.33 Å and a C−S−Ag angle of 107°. Now a partially occupied molecular orbital, as highlighted by a red arrow in Figure 3c, appears at the Fermi energy. The bonding motif of the Ag-linked dimer can be understood by inspecting the wave function of the half-filled orbital at the Fermi energy, which is displayed in panels c_1 and c_2 of Figure 3. The bonding molecular orbital is between the hybridized Ag-d_{xz} and S-p_z atomic orbitals. The latter are bonded with the extended aromatic C-π_p orbitals. The calculated β charges, which partition the exchanged charge density in space, are indicated in Figure 3c_2. The silver atom donates −0.34e, which is equally shared between the two sulfur atoms, as indicated by their β charges of +0.18e. This state expands to a half-filled band with an effective electron mass of $0.12m_e$ in the infinite $[-Ag-S-BP-S-]_n$ chain, which we simulate by applying periodic boundary conditions along the long axis of the molecule (see Figure 3d). In the infinite linear chain, the torsion angle between molecules is reduced to 17°, leading to a nearly flat extended aromatic molecular ribbon. Thus, the −S−Ag−S− linkage leads to a linear polymer that has metallic conductivity, in agreement with the observed conductive sheets in the experiments.

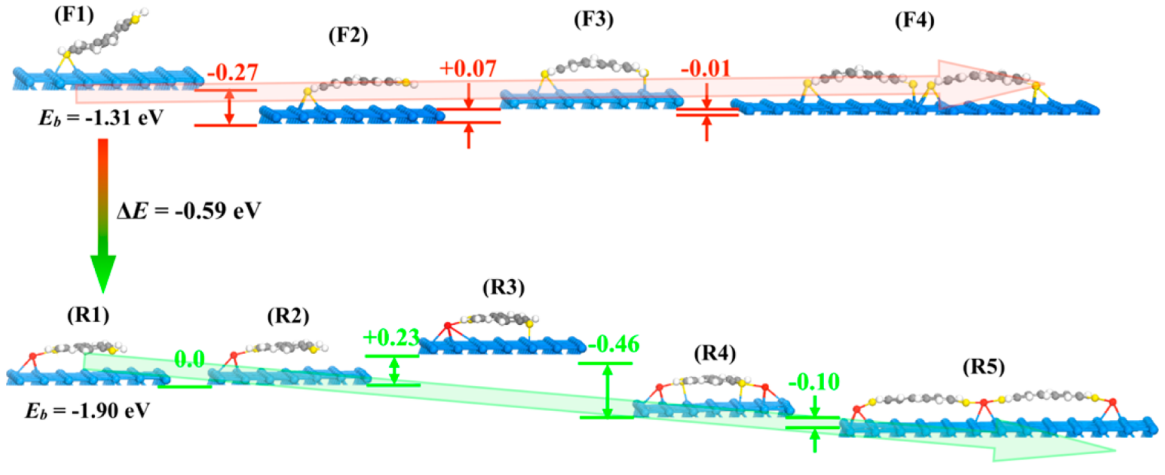

Figure 4. Optimized geometries and energetics (in electronvolts) of BPDT molecules adsorbed on flat (F) and rough (R) Ag(111) surfaces. The yellow, gray, white, and cyan balls in the models are sulfur, carbon, hydrogen, and Ag atoms, respectively. The red ball represents the Ag adatom.

dx.doi.org/10.1021/jp505441k | J. Phys. Chem. C XXXX, XXX, XXX−XXX

Roughness-Catalyzed Polymerization. A careful analysis of the energetics of intermediates in the assembly of the polymer, which is summarized in Figure 4 (also Table S1 of Supporting Information), provides the rationale for the requirement of roughness for its synthesis. Two different sequences are considered. On the flat surface, Figure 4(F1−F4), we assume absence of Ag adatoms, while on the "rough" surface, Figure 4(R1−R5), we assume an ample supply. Where an S−H bond is broken, we assume it to be concerted with H atom adsorption; as such, we use the energies of single Ag and H adatoms on clean Ag(111) as reference states. The stability of various adsorption geometries is determined according to their binding energies

$$E_b = E_{BPDT/Ag(111)} - E_{Ag(111)} - E_{BPDT} \quad (1)$$

where $E_{BPDT/Ag(111)}$ is the total energy of the BPDT/Ag(111) system; $E_{Ag(111)}$ and E_{BPDT} are total energies of the clean or rough Ag(111) surface and an isolated BPDT molecule, respectively.

On the clean surface, the unrelaxed molecule is strongly chemisorbed, with a binding energy of $E_b = -1.31$ eV and an S−Ag(111) bond length of 2.09 Å. After structural relaxation, using the vdW-DF functional, the system gains an additional 0.27 eV by flattening and bending toward the surface. In the process, F1 → F2, the torsion angle reduces from 30° to 7°, the chemisorbed S−Ag bond stretches to 2.13 Å, and the distance between the sulfur atom at the S−H end and the Ag surface shrinks to 2.95 Å. The dehydrogenation of the second thiol, F2 → F3, occurs at a thermally accessible energy cost of 70 meV, to form ionic S−Ag bonds at both ends of the molecule (see Figure S2 of Supporting Information). Remarkably, two dehydrogenated molecules repel each other (F4). Even when we initialize the calculations with two S atoms separated at 2 Å, namely, the S−S bond length of the free dimer, they separate on the surface to an intermolecular S−S distance of 3.8 Å. Thus, even when we start with fully dehydrogenated molecules that are tightly bound to the surface, polymerization does not occur. Consistent with the experiments, BPDT forms a SAM on flat silver.

The chemisorption energy of BPDT on the "rough" surface is increased by ∼0.6 eV ($E_b = -1.9$ eV) through binding to an Ag adatom (R1). Upon structural relaxation (R2), the molecule flattens as before (torsion angle of 3°) and tilts toward the surface, such that the distance between the S and Ag at the S−H end reaches 2.66 Å, while the bonded S−Ag_{ad} distance is 2.5 Å. In the process, the binding of the Ag adatom to the surface is reduced, as evidenced by the change in its vertical height from 2.11 to 2.14 Å, between free and DBDT bound adatom. In the absence of another Ag adatom, the dehydrogenation of the second sulfur is endothermic by 0.23 eV (R2 → R3), while in the presence of the second Ag adatom the process is exothermic by 0.23 eV (R2 → R4). This process should happen readily because at room temperature adatoms are mobile on the silver surface. On Ag (111), the calculated barrier for the diffusion of a Ag atom is 80 meV (cf. Figure S2 of Supporting Information), comparable with the experimental value of 97 ± 10 meV.[16] It appears that Ag adatom bound DBDT molecules are also mobile. Therefore, adatoms with and without molecular cargo readily sample the surface through diffusion. Because the linking of two molecules through the adatom, R3 → R4, is exothermic, we expect the chain to propagate as long as there are mobilized BPDT and Ag atoms on the surface. This provides the mechanistic rationale for the observed roughness-catalyzed polymerization of DBDT on silver. The analyses of the projected density of states and charge density difference of (F3) and (R4) geometries, as shown in Figure S3 of Supporting Information, reveal that the enhanced ionicity in the bonding of BDPT through an Ag adatom is crucial for the attraction between Ag adatom and S atoms, as required for the formation of the continuous chain.

CONCLUSIONS

Metal thiolates, and specifically of coinage metals, show rich structural diversity.[17] Traditionally, silver organo-thiolates are prepared by mixing Ag^+ in solution with the desired thiol, and are known to readily polymerize.[18,19] With alkane monothiols, infinite two-dimensional sheets are formed in which the alkanes are anchored to planes that contain a zigzag arrangement of −S−Ag−S− linked head groups.[20,21] Upon melting, the polymers behave as liquid crystals or covalent soaps.[21] With dithiolates, additional motifs for binding and meso-phase formation have been suggested, with both 2-coordinated and 3-coordinated Ag playing the role of interchain binding.[22] Structural analysis invariably indicates silver atoms that are weakly bonded to multiple sulfurs. In contrast with this standard chemistry, the polymerization we observe occurs on zerovalent silver, Ag^0. Our DFT analysis shows a partial charge of 0.34e on the Ag atoms in the polymer, suggesting a formal valence between 0 and I, in agreement with the XPS analysis. Otherwise, both the observed polymer habit and its primary linear $[-Ag-S-BP-S-]_n$ structure are common motifs in Ag−thiolates. We show that such linear chains lead to near metallic conductivity in a flat ribbon assembly in which the torsion angle between phenyls, which otherwise is a source of resistance to conductivity,[23] is nearly eliminated. The flattening is impressed by extending the π-conjugation between the biphenyl monomers, with the half-filled $-S(p_z)-Ag(d_{xz})-S(p_z)-$ orbital serving as the conductive intermolecular bridge. The long persistence length of flattened molecular wires is consistent with the observed micron-sized 2D sheets as the most common habit of SAP. The sheets are likely to template by the silver surface, as commonly observed in 2D metallo−organic surface assemblies.[24] It is significant that the sheets extrude and continue 3D growth, which we associate with the fact that the 2D polymer sheet and the silver surface have incommensurate meshes (illustrated in Figure S1 of Supporting Information). While the formation of the secondary structure is not addressed, the elementary steps in the polymerization on rough surfaces is clarified and contrasted with flat surfaces by the DFT calculations. In the absence of adatoms, the preference for formation of SAMs is associated with the repulsion between dimers due to the ionicity of the S−Ag bond, which is overcome by the insertion of Ag adatoms that are mobile at room temperature. This general principle of assembly at the metal−liquid interface has also been recognized in related systems, e.g., the linear chain formation near step edges on copper.[25] The simulations predict that long Ag−DBDT chains weakly bound to the surface are the precursors for the 2D secondary structures seen in SEM, and this motif of assembly has a precedent in organo−gold linear chains of 1,4-phenylene diisocyanide seen in STM.[26] While in our modeling we have considered only the Ag[111] surface, we recognize that higher energy surfaces are richer in their adatom supply and may be more efficient in catalyzing the observed polymerization.

The hitherto unknown polymerization of the dithiol on zerovalent Ag is understood to be driven by Ag-adatoms

dx.doi.org/10.1021/jp505441k | J. Phys. Chem. C XXXX, XXX, XXX−XXX

presented by roughened surfaces. The high intrinsic conductvity of the polymers derives from the half-filled band generated by the −S−Ag−S− linkage and planarity of the aromatic π-orbitals enforced by hyperconjugation between Ag-d_{xz} and S-p_z orbitals. The latter effect is recognized in the formation of sheets as the common habit seen through electron microscopy. The facile self-assembly of the polymers, be it as molecular wires or 2D sheets, makes them particularly attractive for applications in bottom-up designs of molecular electronic circuitry.[27] For example, it should be possible to make on-board interconnects by chemical etching of silver contacts or by initiating the catalyzed assembly of the polymers by point defects. More generally, metallic conductive wires and sheets of silver dithio-polymers represent potential alternatives to nanotubes and graphitic sheets in many conceived applications.

■ ASSOCIATED CONTENT

Supporting Information

The main structure and energy parameters of the configurations in Figure 4, analysis of the energetics of intermediates in the assembly of the polymer, the energy barriers of the diffusion of Ag adatom on Ag(111) surface, and experimental and simulated Raman spectroscopy of SAPs. This material is available free of charge via the Internet at http://pubs.acs.org.

■ AUTHOR INFORMATION

Corresponding Authors

*E-mail: aapkaria@uci.edu.

*E-mail: wur@uci.

Present Addresses

[‖]S.S.S.: Department of Chemistry and Biochemistry, UCLA, Los Angeles, CA 90095-1569.

[§]Y.-N.Z.: Chengdu Green Energy and Green Manufacturing Technology R&D Center, Chengdu, 610207, China.

[⊥]P.Z.E.-K.: Physical Sciences Division, Pacific Northwest National Laboratory, P.O. Box 999, Richland, WA 99352.

Notes

The authors declare no competing financial interest.

■ ACKNOWLEDGMENTS

This work was made possible through the unique opportunities granted in the NSF Center for Chemical Innovation on Chemistry at the Space-Time Limit (CaSTL) CHE-0802913. The SEM measurements were performed at the Laboratory for Electron and X-ray Instrumentation (LEXI) at UC Irvine, using instrumentation funded in part by CaSTL (CHE-0802913). We are indebted to Prof. M. Law for his guidance and directorship of LEXI. We also thank Dr. Joonhee Lee for many helpful discussions.

■ REFERENCES

(1) Song, Z.; Zhou, H. Towards Sustainable and Versatile Energy Storage Devices: An Overview of Organic Electrode Materials. *Energy Environ. Sci.* **2013**, *6*, 2280.

(2) Takamatsu, S.; Kurihara, K.; Yamashita, T.; Itoh, T. Simple Micro-Patterning of High Conductive Polymer with UV-Nano-Imprinted Patterned Substrate and Ethylene Glycol-Based Second Doping. *J. Micromech. Microeng.* **2014**, *24*, 045024.

(3) Tuccitto, N.; Ferri, V.; Cavazzini, M.; Quici, S.; Zhavnerko, G.; Licciardello, A.; Rampi, M. A. Highly Conductive Approximately 40-nm-Long Molecular Wires Assembled by Stepwise Incorporation of Metal Centres. *Nat. Mater.* **2009**, *8*, 41−46.

(4) Maeda, H.; Sakamoto, R.; Nishihara, H. Metal Complex Oligomer and Polymer Wires on Electrodes: Tactical Constructions and Versatile Functionalities. *Polymer* **2013**, *54*, 4383−4403.

(5) Chiang, C.; Fincher, C.; Park, Y.; Heeger, A.; Shirakawa, H.; Louis, E.; Gau, S.; MacDiarmid, A. Electrical Conductivity in Doped Polyacetylene. *Phys. Rev. Lett.* **1977**, *39*, 1098−1101.

(6) Chiang, C. K.; Druy, M. A.; Gau, S. C.; Heeger, A. J.; Louis, E. J.; MacDiarmid, A. G.; Park, Y. W.; Shirakawa, H. Synthesis of Highly Conducting Films of Derivatives of Polyacetylene, $(CH)_x$. *J. Am. Chem. Soc.* **1978**, *100*, 1013−1015.

(7) Bachtold, A.; Hadley, P.; Nakanishi, T.; Dekker, C. Logic Circuits with Carbon Nanotube Transistors. *Science* **2001**, *294*, 1317−1320.

(8) Frank, S. Carbon Nanotube Quantum Resistors. *Science* **1998**, *280*, 1744−1746.

(9) Hermosa, C.; Vicente Álvarez, J.; Azani, M.-R.; Gómez-García, C. J.; Fritz, M.; Soler, J. M.; Gómez-Herrero, J.; Gómez-Navarro, C.; Zamora, F. Intrinsic Electrical Conductivity of Nanostructured Metal-Organic Polymer Chains. *Nat. Commun.* **2013**, *4*, 1709.

(10) Lu, W.; Lieber, C. M. Nanoelectronics from the Bottom Up. *Nat. Mater.* **2007**, *6*, 841−850.

(11) Love, J. C.; Estroff, L. A.; Kriebel, J. K.; Nuzzo, R. G.; Whitesides, G. M. Self-Assembled Monolayers of Thiolates on Metals as a Form of Nanotechnology. *Chem. Rev. (Washington, DC, U.S.)* **2005**, *105*, 1103−1169.

(12) Blum, A. S.; Kushmerick, J. G.; Long, D. P.; Patterson, C. H.; Yang, J. C.; Henderson, J. C.; Yao, Y.; Tour, J. M.; Shashidhar, R.; Ratna, B. R. Molecularly Inherent Voltage-Controlled Conductance Switching. *Nat. Mater.* **2005**, *4*, 167−172.

(13) Shirakawa, H.; Louis, E. J.; MacDiarmid, A. G.; Chiang, C. K.; Heeger, A. J. Synthesis of Electrically Conducting Organic Polymers: Halogen Derivatives of Polyacetylene, (CH) X. *J. Chem. Soc., Chem. Commun.* **1977**, 578.

(14) Pauly, F.; Viljas, J.; Cuevas, J.; Schön, G. Density-Functional Study of Tilt-Angle and Temperature-Dependent Conductance in Biphenyl Dithiol Single-Molecule Junctions. *Phys. Rev. B: Condens. Matter Mater. Phys.* **2008**, *77*, 155312.

(15) Mishchenko, A.; Vonlanthen, D.; Meded, V.; Bürkle, M.; Li, C.; Pobelov, I. V.; Bagrets, A.; Viljas, J. K.; Pauly, F.; Evers, F.; et al. Influence of Conformation on Conductance of Biphenyl-Dithiol Single-Molecule Contacts. *Nano Lett.* **2010**, *10*, 156−163.

(16) Brune, H.; Bromann, K.; Röder, H.; Kern, K.; Jacobsen, J.; Stoltze, P.; Jacobsen, K.; Nørskov, J. Effect of Strain on Surface Diffusion and Nucleation. *Phys. Rev. B: Condens. Matter Mater. Phys.* **1995**, *52*, R14380−R14383.

(17) Duran, N.; Clegg, W.; Fraser, K. A.; González-Duarte, P. The Reaction Chemistry of 2- and 3-Aminoalkanethiols with $[PtMe_3I]_4$: A New Example of the Structural Diversity of Metal Thiolates. *Inorg. Chim. Acta* **2000**, *300*−*302*, 790−799.

(18) Akerstrom, S. Silver(I) Alkanethiolates. *Ark. Kemi* **1965**, *24*, 505.

(19) Bell, R. A.; Kramer, J. R. Structural Chemistry and Geochemistry of Silver-Sulfur Compounds: Critical Review. *Environ. Toxicol. Chem.* **1999**, *18*, 9−22.

(20) Dance, I. G.; Fisher, K. J.; Banda, R. M. H.; Scudder, M. L. Layered Structure of Crystalline Compounds Silver Thiolates (AgSR). *Inorg. Chem.* **1991**, *30*, 183−187.

(21) Baena, M. J.; Espinet, P.; Lequerica, M. C.; Levelut, A. M. Mesogenic Behavior of Silver Thiolates with Layered Structure in the Solid State: Covalent Soaps. *J. Am. Chem. Soc.* **1992**, *114*, 4182−4185.

(22) Fijolek, H. G.; González-Duarte, P.; Park, S. H.; Suib, S. L.; Natan, M. J. Structure−Spectroscopy Correlations in Silver Thiolates: Application to the Structure of Silver 1,5-Pentanedithiolate. *Inorg. Chem.* **1997**, *36*, 5299−5305.

(23) Bürkle, M.; Viljas, J. K.; Vonlanthen, D.; Mishchenko, A.; Schön, G.; Mayor, M.; Wandlowski, T.; Pauly, F. Conduction Mechanisms in Biphenyl Dithiol Single-Molecule Junctions. *Phys. Rev. B: Condens. Matter Mater. Phys.* **2012**, *85*, 075417.

(24) Tait, S. L.; Langner, A.; Lin, N.; Chandrasekar, R.; Fuhr, O.; Ruben, M.; Kern, K. Assembling Isostructural Metal-Organic

Coordination Architectures on Cu(100), Ag(100) and Ag(111) Substrates. *ChemPhysChem* **2008**, *9*, 2495−2499.
(25) Tait, S. L.; Langner, A.; Lin, N.; Stepanow, S.; Rajadurai, C.; Ruben, M.; Kern, K. One-Dimensional Self-Assembled Molecular Chains on Cu(100): Interplay between Surface-Assisted Coordination Chemistry and Substrate Commensurability. *J. Phys. Chem. C* **2007**, *111*, 10982−10987.
(26) Zhou, J.; Acharya, D.; Camillone, N.; Sutter, P.; White, M. G. Adsorption Structures and Electronic Properties of 1,4-Phenylene Diisocyanide on the Au(111) Surface. *J. Phys. Chem. C* **2011**, *115*, 21151−21160.
(27) Kwiat, M.; Cohen, S.; Pevzner, A.; Patolsky, F. Large-Scale Ordered 1D-Nanomaterials Arrays: Assembly or Not? *Nano Today* **2013**, *8*, 677−694.
(28) Sasaki, S. S.; Perdue, S. M.; Perez, A. R.; Tallarida, N.; Majors, J. H.; Apkarian, V. A.; Lee, J. Note: Automated Electrochemical Etching and Polishing of Silver Scanning Tunneling Microscope Tips. *Rev. Sci. Instrum.* **2013**, *84*, 096109.
(29) Lindberg, B. J.; Hamrin, K.; Johansson, G.; Gelius, U.; Fahlman, A.; Nordling, C.; Siegbahn, K. Molecular Spectroscopy by Means of ESCA II. Sulfur Compounds. Correlation of Electron Binding Energy with Structure. *Phys. Scr.* **1970**, *1*, 286−298.
(30) NIST X-ray Photoelectron Spectroscopy Database, version 4.1. http://srdata.nist.gov/xps/ (accessed Apr 15, 2014).
(31) Kresse, G.; Furthmüller, J. Efficiency of Ab-Initio Total Energy Calculations for Metals and Semiconductors Using a Plane-Wave Basis Set. *Comput. Mater. Sci.* **1996**, *6*, 15−50.
(32) Blöchl, P. E. Projector Augmented-Wave Method. *Phys. Rev. B: Condens. Matter Mater. Phys.* **1994**, *50*, 17953−17979.
(33) Perdew, J. P.; Burke, K.; Ernzerhof, M. Generalized Gradient Approximation Made Simple. *Phys. Rev. Lett.* **1996**, *77*, 3865−3868.
(34) Klimeš, J.; Bowler, D. R.; Michaelides, A. Van Der Waals Density Functionals Applied to Solids. *Phys. Rev. B: Condens. Matter Mater. Phys.* **2011**, *83*, 195131.